

Article

Luminescence Properties of Fe²⁺:ZnSe Single Crystals Grown via a Traveling Heater Method

Weina Nan, Da Yang, Boru Zhou *, Liang Zhang, Jing Xiao, Hongwei Yu, Zhanggui Hu and Yicheng Wu

Tianjin Key Laboratory of Functional Crystal Materials, Institute of Functional Crystals, School of Materials Science and Engineering, Tianjin University of Technology, Tianjin 300384, China

* Correspondence: zhoubr@email.tjut.edu.cn

Abstract: The luminescence properties of iron-doped ZnSe (Fe²⁺:ZnSe) single crystals grown via a traveling heater method have been studied via photoluminescence (PL). Nine emission bands were identified in the PL spectra of Fe²⁺:ZnSe single crystals and their origins were also discussed. The near-infrared emission bands seen at 820 nm and 978 nm can be attributed to the emission bands formed by the background Fe or other impurity-related defect complexes in Fe²⁺:ZnSe single crystals, rather than by doped transition-metal-related defects. With the increase in temperature, the PL intensity increased slightly and reached a maximum near room temperature for bound excitons (430–490 nm), but the PL intensity decreased significantly for impurity-defect emission bands (500–720 nm), indicating the occurrence of a thermal quenching effect. The excitation wavelength-dependent PL spectra showed that PL intensity first increased and then decreased with an increase in the excitation wavelengths, and the maximum PL intensity of the bound excitons was obtained at 364 nm. In addition, the X-ray photoelectron spectroscopy (XPS) results showed that both bivalent and trivalent iron ions were found, but bivalence was the dominant charge state for iron atoms in the iron-doped ZnSe single crystals, meaning that they are suitable for developing mid-infrared gain medium applications.

Keywords: Fe²⁺:ZnSe; photoluminescence; defects; traveling heater method; single crystals; mid-infrared laser



Citation: Nan, W.; Yang, D.; Zhou, B.; Zhang, L.; Xiao, J.; Yu, H.; Hu, Z.; Wu, Y. Luminescence Properties of Fe²⁺:ZnSe Single Crystals Grown via a Traveling Heater Method. *Crystals* **2023**, *13*, 411. <https://doi.org/10.3390/cryst13030411>

Academic Editors: Alessandra Toncelli, Kai Zhong, Xinyuan Zhang and Pengxiang Liu

Received: 3 February 2023

Revised: 19 February 2023

Accepted: 21 February 2023

Published: 27 February 2023



Copyright: © 2023 by the authors. Licensee MDPI, Basel, Switzerland. This article is an open access article distributed under the terms and conditions of the Creative Commons Attribution (CC BY) license (<https://creativecommons.org/licenses/by/4.0/>).

1. Introduction

As in recent decades, the wide-bandgap semiconductor, zinc selenide (ZnSe), and its solid solution are still of intense interest due to their promising application in high-performance photoelectric devices [1–4]. Especially in the case of transition-metal iron-doped ZnSe crystals (Fe²⁺:ZnSe), they generally exhibit broad tunability, low optical losses, great absorption, and emission cross-sections in the mid-infrared range of 3–5 μm [5–7], and have been considered as one of the most promising mid-infrared gain materials for applications in lasers, molecular spectroscopy, space-based remote sensing, atmospheric monitoring, etc. For these applications, it is important to understand the nature as well as the basic properties of intrinsic defects, impurities, and their complex defects for obtaining a high-performance Fe²⁺:ZnSe-based active gain medium. Firstly, the photoelectrical properties of the grown crystals depend not only on intrinsic defects (interstitials, vacancies, anti-sites) but also on impurities derived from intentional/unintentional dopants during crystal growth [8]. Secondly, impurity-related defect states can also be used to develop new Fe²⁺:ZnSe laser systems [9,10].

Photoluminescence (PL) is a sensitive and non-destructive characterization technique to investigate intrinsic defects, impurities, and complex defects in semiconductor materials [11–13]. For the PL spectra of ZnSe crystals, two regions have been identified: the near-band edge emission, associated with free and bound excitons (the blue spectral region), and the emission spectra related to impurity-defect complexes (the range from green to red spectral regions). Regarding these emission spectra, different origins have been discussed and ascribed to intrinsic point defects and their complexes with impurities, such

as zinc vacancies [14], zinc interstitials [15], selenium vacancies [16], and A centers (V_{Zn} -Cu complex centers [8], etc.). For example, Avetissov et al. [8] investigated the PL of ZnSe crystals grown using different techniques (the high-pressure melt method, physical vapor transport (PVT), and chemical vapor deposition (CVD)) at room temperature. They found that the emission peaks at 2.1 eV and 2.13 eV could be attributed to an excess of Se in ZnSe crystals, while the peaks at 2.42 eV and 2.48 eV were associated with an excess of Zn. Sushkevich et al. [17] observed the maximum emission peak at 570–580 nm on the PL spectra of ZnSe crystals doped with antimony and iodine; they attributed the emission peak to the Sb_{Se} - I_{Se} complex center with an energy level located at 0.5 eV above the valence band maximum. The PL spectra of polycrystalline Fe^{2+} :ZnSe, prepared by the thermal diffusion method, were also studied at low temperatures [18], wherein a new stable defect complex with a narrow emission line at 0.681 eV was temporarily attributed to an intra-center transition formed by the doped-iron ion and an intrinsic point defect (a Zn vacancy), while the emission lines in the range of 1.4–2.8 eV were dominated by background impurities or intrinsic point defects, and those in the range of 1.28–1.31 eV were associated with an iron-related complex defect [19]. Moreover, Gladilin et al. [20] studied the PL spectra of polycrystalline Fe^{2+} :ZnSe with different iron-ion concentrations. The results showed the formation of auxiliary luminescence bands, including the luminescence of residual tetrahedral donors and acceptors, an unknown bound exciton line located at 459 nm, broad bands with maxima at 490, 520, 670, and 820 nm, and an IR band at 960 nm. The emission lines in the range of 1.30–2.76 eV were only associated with intrinsic defects and/or impurities, not with the optically active iron ion. The PL spectra of Fe^{2+} :ZnSe single crystals at room temperature also showed that a high iron concentration would result in an increase in the degree of inhomogeneity in ZnSe crystals and then cause low-intensity luminescence emissions [21]. The mid-IR luminescence of Fe^{2+} ions in ZnSe under visible excitation was also studied by Peppers et al. [9], wherein a near-IR PL at 950 nm with a decay time of 49 μ s was observed, but its origin was not discussed. In addition, the electronic structures of ZnSe crystals with various point defects were also calculated by Hizhnyi et al. [22] by using the plane-wave pseudopotential method within the DFT approximation, which yields the ionization energies of native (Zn_i , V_{Zn} , V_{Se} , and their complexes) and doping-related point defects (Al_{Zn} , Te_{Se} , O_{Se} , and their complexes) and is helpful for understanding the point defects and defects-related luminescence properties of doped/undoped ZnSe crystals.

Although numerous studies have focused on the luminescence properties of doped/undoped ZnSe crystals that have been prepared by the melt method, the thermal diffusion method, PVT, and CVD, the luminescence properties of Fe^{2+} :ZnSe single crystals grown via the traveling heater method and using a high-temperature solvent have not been studied, to the best of our knowledge. In the present work, we report the luminescent properties of Fe^{2+} :ZnSe single crystals grown via the traveling heater method. The origins and identifications of impurity- and defect-related emission bands in the Fe^{2+} :ZnSe crystals were determined, and the excitation wavelengths- and temperature-dependent PL spectra were investigated. In addition, the transmittance to the infrared band of Fe:ZnSe crystals and the charge states of the Fe atoms in them were also evaluated via an infrared spectrometer and X-ray photoelectron spectroscopy.

2. Materials and Methods

For crystal growth, the quartz ampoule was first washed with acetone, aqua regia, and deionized water in turn and was then coated with a uniform carbon film inside the quartz ampoule. SnSe (5N), FeSe (3N), and CVD-grown polycrystalline ZnSe with 5N purity were loaded in order into the carbon-coated quartz ampoule, which was then sealed under a vacuum of 4×10^{-5} Pa using an H_2 - O_2 torch. The crucible was loaded into a self-designed six-zone growth furnace, then the program was run to grow iron-doped ZnSe crystals, as described in detail in Ref. [23]. Finally, the iron-doped ($\sim 10^{19}$ cm^{-3}) and undoped ZnSe single-crystal samples were prepared via the traveling heater method.

Before various tests, the samples were mechanically polished, using a suspension of alumina powders with an average size of 1 micron, then washed in acetone and deionized water. The PL spectra were measured in a temperature range from 77 K to 438 K using a fluorescence spectrometer (FLS-980, Edinburgh, UK). A 450 W xenon arc lamp was employed as a continuous excitation light source. The FLS980 spectrometer was configured with two photomultipliers: a thermos-electrically cooled red photomultiplier (Red PMT) with spectral coverage from 200 nm to 870 nm and a liquid nitrogen cooled near-infrared photomultiplier (NIR-PMT) with spectral coverage from 500 nm to 1700 nm. A liquid nitrogen-cooled cryostat (Optistat DN, OXFORD instruments, Oxford, UK) with a temperature range from 77 K to 500 K was used to obtain PL spectra at different temperatures. A deconvolution method (Gaussian fitting) is commonly used for qualitative analysis in the previous literature [16,24,25], although this method is tentative for analyzing PL spectra. Herein, combined with the reported emission bands, the deconvolution method was utilized to analyze the emission bands in the PL spectra of ZnSe:Fe²⁺ single crystals. In addition, a Nicolet iS50 spectrometer (ThermoFisher, Waltham, MA, USA) with a scanning range of 400–4000 cm⁻¹ and a UV-Vis-NIR spectrophotometer (UH4150, HITACHI, Tokyo, Japan) with a scanning range of 190–2500 nm were employed to study the infrared transmittance and the band-gap absorption edge of the samples. X-ray photoelectron spectroscopy (XPS, EscaLab 250Xi, ThermoFisher, Waltham, MA, USA) was utilized to determine the charge states of doped iron atoms in the ZnSe crystals.

3. Results and Discussion

Figure 1 shows the transmittance spectrum of Fe²⁺:ZnSe single crystals grown via the traveling heater method. The average transmittance reached 70%, which is comparable to high-quality crystals [26]. The absorption cutoff edge was around 475 nm and its corresponding energy was higher than the bandgap energy of 2.54 eV for undoped ZnSe crystals at room temperature. The absorption cutoff edge shifted toward the shorter wavelength because of the electron transitions among the different energy states of the iron ions in the ZnSe crystals. A wide-band and strong absorption of around 3 μm was observed in the transmittance spectrum, which corresponded to the ⁵E(D) → ⁵T₂(D) transition within the 3d⁶ shells of Fe²⁺ ions [27]. In addition, dislocation etch pits were observed on the ZnSe(110) cleavage plane, etched with 40% NaOH aqueous solution at 95 °C for 60 min; the etch pit density (EPD) was as high as 1.85 × 10⁶ cm⁻², as shown in Figure 1b.

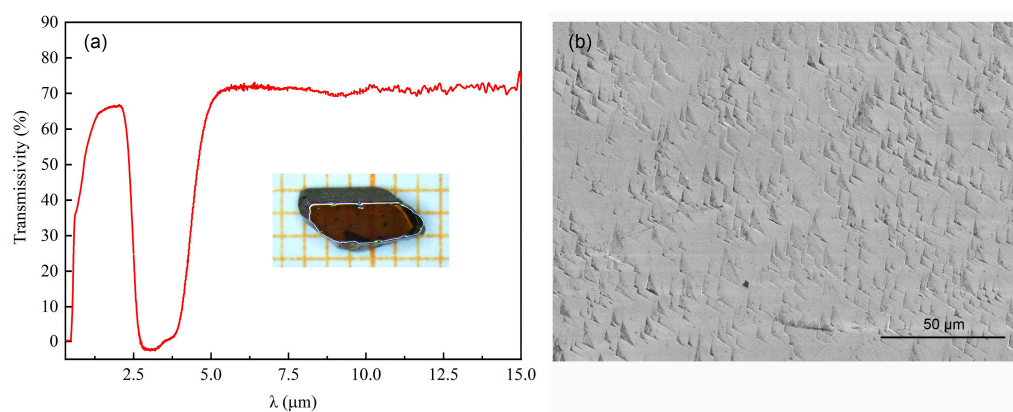


Figure 1. The transmittance spectrum and dislocation etch pits of Fe²⁺:ZnSe single crystals grown via the traveling heater method: (a) the transmittance spectrum of the Fe²⁺:ZnSe sample; (b) the dislocation etch pits on the ZnSe(110) cleavage plane. The inset shows a photograph of polished Fe²⁺:ZnSe single crystals.

XPS measurements were performed to study the chemical states of Fe atoms in iron-doped ZnSe single crystals. Before the XPS measurements, a sputtering technique using Ar⁺ ion bombardment was used to remove contaminants from the surface of iron-doped ZnSe

single crystals. The high-resolution XPS spectra of Zn, Se, Fe, and iron-doped ZnSe single crystals are shown in Figure 2. Two main peaks with binding energies of 1022.3 eV and 1045.5 eV were observed in the XPS spectrum of Zn 2p (Figure 2a); these were attributed to Zn 2p_{3/2} and Zn 2p_{1/2} orbitals and indicated the existence of Zn²⁺ [28]. The binding energy of Se 3d was determined to be 54.8 eV (Figure 2b), corresponding to the characteristic value of Se²⁻ [29]. The binding energies at 710.4 eV and 724.1 eV could be determined from the XPS spectrum of Fe 2p (Figure 2c), which corresponded to Fe 2p_{3/2} and Fe 2p_{1/2} orbitals, respectively [30]. The main Fe 2p_{3/2} peak exhibits associated satellite peaks, which are used to distinguish the charge states of Fe atoms in compound materials [31]. In an XPS spectrum of Fe 2p, two satellite peaks can also be observed at 716.1 eV and 720.1 eV, respectively. Satellite peak 1, with a binding energy of 716.1 eV, offers clear evidence for the existence of Fe²⁺. Satellite peak 2, with a binding energy of 720.1 eV, can be assigned to the characteristic peaks of Fe³⁺; its peak intensity is very weak compared with satellite peak 1, which indicates that the amount of Fe³⁺ is extremely small in the iron-doped ZnSe matrix. Although the surface of the iron-doped ZnSe sample was etched for 30 s via Ar⁺ ion bombardment, which works well for the removal of loosely bound adsorbed species, the stable Fe³⁺ ions oxidized on the iron-doped ZnSe matrix surface were not completely removed. The results show that the iron ions with bivalent charge states are dominant in the iron-doped ZnSe matrix. The XPS spectrum of iron-doped ZnSe single crystals is shown in Figure 2d. It can be seen that the characteristic peaks of Fe were not as strong as those of the matrix element (Zn and Se), indirectly indicating that iron ions are homogeneous in the ZnSe matrix. Combined with a characteristic absorption peak around 3 μm in the infrared transmittance spectrum (Figure 1), this confirmed that the dominant iron ions with divalent charge states were successfully incorporated into the ZnSe single crystals.

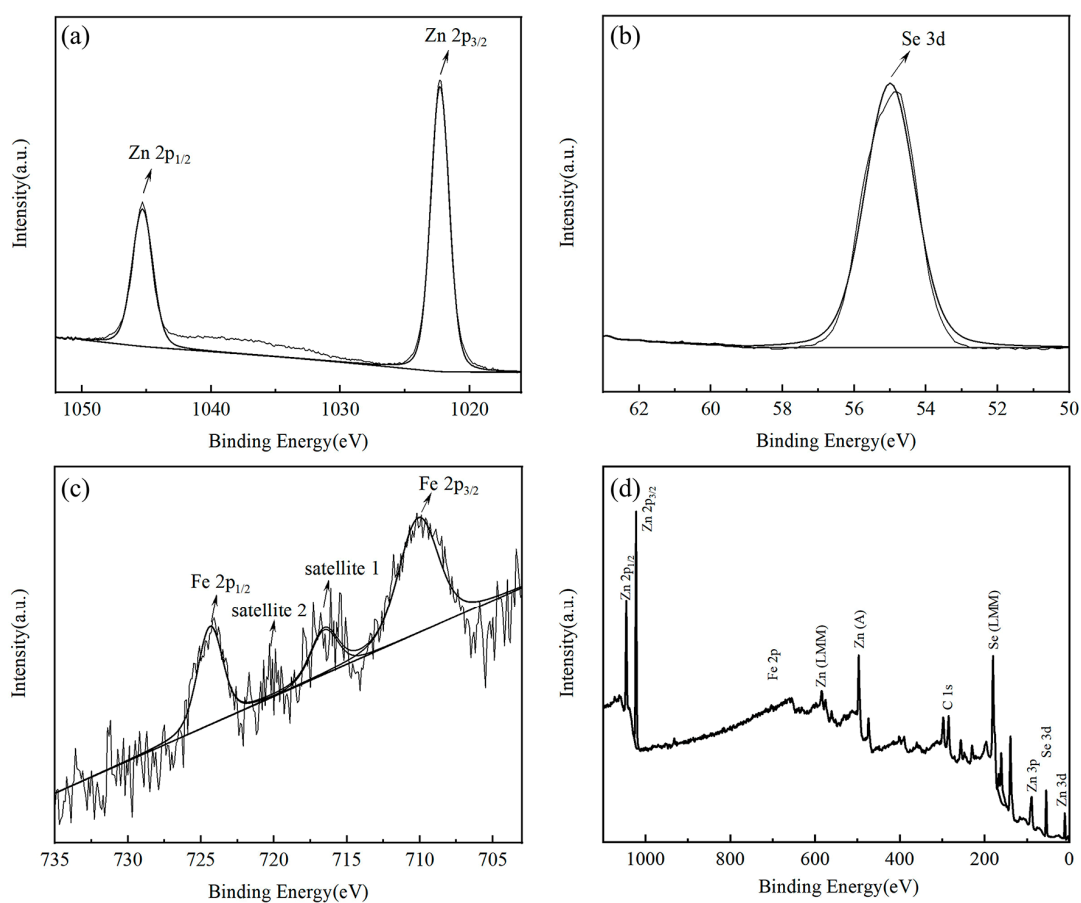


Figure 2. The XPS spectra of Fe²⁺:ZnSe single crystals after etching for 30 s. (a) Zn element, (b) Se element, (c) Fe element, (d) the total spectrum of Fe²⁺:ZnSe single crystals.

Figure 3 shows the typical PL spectra of iron-doped and undoped ZnSe single crystals grown using the traveling heater method. In the PL spectra, three types of luminescence emissions can be distinguished: an intense emission region in the range of 430–490 nm (the blue bands), a weak emission region in the range of 500–580 nm (the green bands), and a broad emission region in the range of 600–720 nm (the red bands). The blue emission bands are usually attributed to the emission of bound excitons, while the green and red emission bands are related to the emission of impurity-defect complexes [13,20,21]. Compared with the undoped ZnSe sample, intense bound exciton luminescence (the blue bands) at room temperature was observed in the Fe^{2+} :ZnSe single crystals, which indicated that Fe^{2+} :ZnSe single crystals grown via the traveling heater method had high purity and few native/impurity-related defects [8,32]. Nevertheless, for Fe^{2+} :ZnSe single crystals, the PL intensity of the broad emission bands (the green and red bands) between 550 nm and 750 nm was much lower than those of the undoped ZnSe sample, which is consistent with previous studies [21,33]. The results indicated that the incorporation of Fe at high concentrations ($\sim 10^{19} \text{ cm}^{-3}$) in ZnSe crystals resulted in a significant reduction in PL intensity for impurity-defect-related emission bands. Firstly, after doping Fe, Fe and its defect complexes only acted as centers of nonradiative recombination rather than luminescent centers in ZnSe crystals. Secondly, the doped Fe occupied the lattice sites of Zn in ZnSe crystals and resulted in a reduction in Zn vacancies in the ZnSe crystals, followed by a reduction in the emission bands of the impurity-defect complexes associated with Zn vacancies [16]. This finding was further confirmed by M. Surma and M. Godlewski's results, showing that the PL intensity of impurity-defect-related emission bands decreased dramatically with an increase in iron-doped concentration in ZnSe crystals [34].

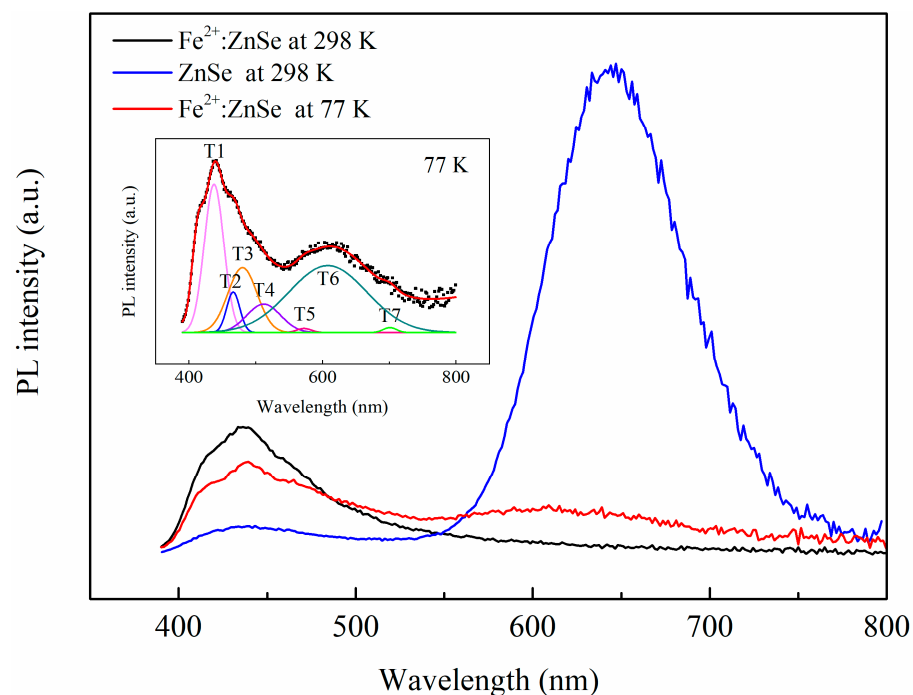


Figure 3. The photoluminescence (PL) spectra of Fe^{2+} :ZnSe single crystals grown via the traveling heater method, measured under an excitation wavelength of 360 nm at room temperature and at a low temperature, respectively. The inset shows the results of Gaussian fitting.

For Fe^{2+} :ZnSe single crystals, seven emission bands (labeled T1–T7) were revealed by the Gaussian fitting, as shown in the inset in Figure 3. The T1 peak at 437 nm was assigned to the emission of excitons bound to neutral donors ($\text{Al}_{\text{Zn}}, \text{In}_{\text{Zn}}$) [35] to excitons bound to charge donors (Cl_{Se}) [35] or neutral acceptors ($\text{P}_{\text{Se}}, \text{N}_{\text{Se}}, \text{Ag}_{\text{Zn}}$) [36,37]. The T2 peak at 466 nm could be attributed to the emission of donor-acceptor pairs (DAP), caused

by a nitrogen-related acceptor [38] or associated with hydrogen-like impurities [20]. The T3 peak in the region of ~ 476 nm was allied to the emissions from dislocations in ZnSe crystals [20,39], often associated with grain boundaries in polycrystalline ZnSe [40]. Hence, for $\text{Fe}^{2+}:\text{ZnSe}$ single crystals with high dislocation density ($1.85 \times 10^6 \text{ cm}^{-2}$), this T3 peak was more likely to be attributable to the emissions associated with a dislocation. The origins of these emission bands, T4–T7, have been studied extensively but remain unclear. The T4–T6 peaks at 512 nm, 572 nm and 608 nm could be attributed to the emissions of chlorine donor-vacancy recombination (Cl-V_{Zn} complex), or to the defect-complexes formed by intrinsic point defects ($\text{Zn}_i, \text{V}_{\text{Zn}}$) and Cu/oxygen/other background impurities [16,21,41]. Finally, the emission band, T7, with its maximum at 700 nm can be attributed to deep centers related to a background As impurity (As_{Se} acceptor) [42].

The PL spectra of the iron-doped and undoped ZnSe single crystals were studied in the near-infrared spectrum region, as shown in Figure 4. Two new emission bands (T8–T9) with a maximum at 820 nm and 978 nm, respectively, were obtained via Gaussian fitting. The identification of these two peaks (T8 and T9) is still an open topic in the context of $\text{Fe}^{2+}:\text{ZnSe}$ crystals. The T9 peak at ~ 978 nm in the PL spectra of $\text{Fe}^{2+}:\text{ZnSe}$ crystals have been ascribed to the emission transition ${}^3\text{T}_1 \rightarrow {}^5\text{E}$ of Fe^{2+} ions in Refs. [9,19]. In contrast, an electron-spin-resonance (ESR) study of iron-doped ZnSe crystals indicated that Fe^{3+} was responsible for an emission band with its maximum at 980 nm [34]. In addition, the luminescence and ESR studies for $\text{Fe}:\text{ZnS}$ crystals showed that Fe^{3+} ions were considered as an emission center to account for the emission band at 980 nm [43]. However, this peak at ~ 978 nm was observed in both iron-doped and -undoped ZnSe single crystals, and its integrated intensity was greater in the iron-undoped sample compared with the iron-doped sample. Therefore, we believe that the luminescence peak at ~ 978 nm is not related to the emission band involving the doped iron atoms but may, instead, be associated with the emission band formed by the background Fe/another impurity-related defect complexes in ZnSe crystals. By the same token, we tentatively attribute the emission peak with a maximum at 820 nm to the emission band associated with background impurity-defect complexes, although it has previously been assigned to the emission transitions associated with Fe^{2+} levels [33].

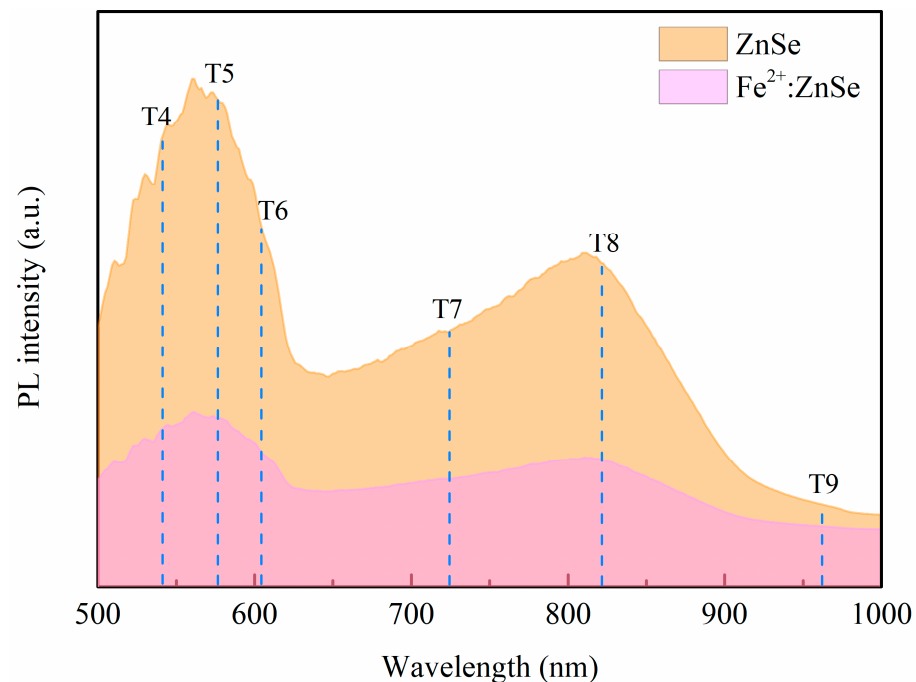


Figure 4. The PL spectra of the iron-doped and undoped ZnSe crystals in the near-infrared spectral region, measured under an excitation wavelength of 480 nm at room temperature.

Figure 5 shows the dependence of the PL spectra of $\text{Fe}^{2+}:\text{ZnSe}$ single crystals on temperature and excitation wavelengths. With an increase in temperature, the PL intensity increased slightly and reached a maximum near room temperature for bound excitons (the blue bands, T1–T3 peaks), but the PL intensity decreased significantly for the impurity-defect emission bands (the green and red bands, T4–T7 peaks), as shown in Figure 5a. These results indicated that the thermal quenching effect of impurity-defect emission bands occurred in the temperature-dependent PL spectra. Various transition mechanisms leading to the thermal quenching of long-wavelength PL in iron-doped ZnSe/ZnS crystals were previously discussed in Refs. [34,44]. However, for bound excitons (the blue bands, T1–T3 peaks), the thermal quenching effect was not observed with an increase in temperatures, which might be due to the high quality (high purity and few native/impurity-related defects) of $\text{Fe}^{2+}:\text{ZnSe}$ single crystals, resulting in strongly bound exciton emissions [8,32]. In addition, it was found that their PL intensity first increased and then decreased with an increase in the excitation wavelength for the bound exciton emission bands (T1–T3 peaks); the maximum PL intensity of bound excitons was obtained at 364 nm, as shown in Figure 5b. For impurity-defect emission bands, their PL intensity increased with an increase in the excitation wavelengths, as shown in Figure 5c.

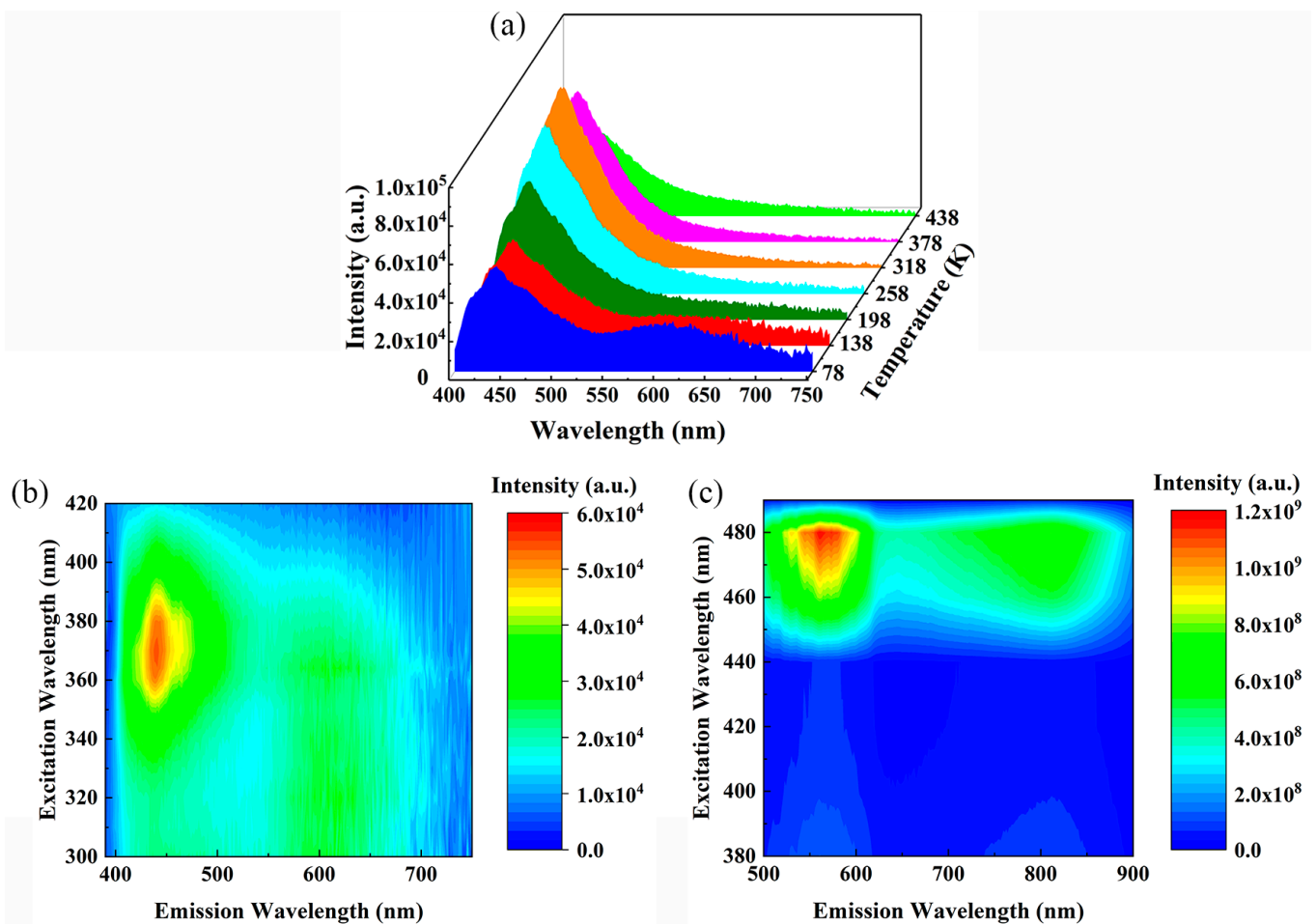


Figure 5. The dependence of PL spectra of $\text{Fe}^{2+}:\text{ZnSe}$ single crystals on temperatures and excitation wavelengths: (a) the temperature-dependence of PL spectra; (b,c) the excitation wavelength dependence of PL spectra at 78 K.

4. Conclusions

In this work, the photoluminescence of $\text{Fe}^{2+}:\text{ZnSe}$ single crystals grown by the traveling heater method was studied and a total of nine emission bands (T1–T9) were identified.

It was found that, for the emission bands (T1–T3) associated with bound excitons, the thermal quenching effect was not observed with the increase in temperature, which might be due to the high quality of the Fe²⁺:ZnSe single crystals resulting in strong bound exciton emissions, while that effect was clearly observed for impurity/defect-related emission bands (T4–T7). For the bound exciton emission bands, PL intensity increased first and then decreased with the increase in the excitation wavelengths, while the maximum PL intensity of bound excitons was obtained at 364 nm. For impurity/defect emission bands, PL intensity increased with the increase in excitation wavelengths. Furthermore, the emission bands (T8–820 nm, T9–980 nm) in the near-infrared region were considered independent of the doped iron atoms and may be associated with the emission band formed by the background Fe/other impurity-related defect complexes in Fe²⁺:ZnSe single crystals. The results of the XPS studies show that both bivalent and trivalent iron ions were found in the iron-doped ZnSe single crystals, but the bivalent charge states were dominant for the iron atoms. The iron ions with divalent charge states have been successfully incorporated into the ZnSe single-crystal matrix.

Author Contributions: Methodology, W.N. and B.Z.; investigation, D.Y. and J.X.; validation, W.N. and B.Z.; data curation, D.Y. and L.Z.; writing—original draft preparation, W.N.; writing—review and editing, B.Z. and H.Y.; project administration, B.Z., Z.H. and Y.W. All authors have read and agreed to the published version of the manuscript.

Funding: This work was supported by the National Natural Science Foundation of China (grant numbers 51902224, 51890864, and 51890865).

Institutional Review Board Statement: Not applicable.

Informed Consent Statement: Not applicable.

Conflicts of Interest: The authors declare that they have no conflict of interest.

References

1. Setera, B.; Su, C.H.; Arnold, B.; Choa, F.S.; Kelly, L.; Sood, R.; Singh, N.B. Comparative study of bulk and nanoengineered doped ZnSe. *Crystals* **2022**, *12*, 71. [\[CrossRef\]](#)
2. Karki, K.; Yu, S.Q.; Fedorov, V.; Martyshkin, D.; Subedi, S.; Wu, Y.Q.; Mirov, S. Hot-pressed ceramic Fe:ZnSe gain-switched laser. *Opt. Mater. Express* **2020**, *10*, 3417–3423. [\[CrossRef\]](#)
3. Galkin, S.; Rybalka, I.; Sidelnikova, L.; Voloshinovskii, A.; Kraus, H.; Mykhaylyk, V. Performance of ZnSe-based scintillators at low temperatures. *J. Lumin.* **2021**, *239*, 118360. [\[CrossRef\]](#)
4. Sirkeli, V.P.; Yilmazoglu, O.; Hajo, A.S.; Nedeoglo, N.D.; Nedeoglo, D.D.; Preu, S.; Küppers, F.; Hartnagel, H.L. Enhanced responsivity of ZnSe-based metal-semiconductor-metal near-ultraviolet photodetector via impact ionization. *Phys. Status Solidi R.* **2018**, *12*, 1700418. [\[CrossRef\]](#)
5. Ruan, P.; Pan, Q.K.; Alekseev, E.E.; Kazantsev, S.Y.; Mashkovtseva, L.S.; Mironov, Y.B.; Podlesnikh, S.V. Performance improvement of a Fe²⁺:ZnSe laser pumped by non-chain pulsed HF laser. *Optik* **2021**, *242*, 167005. [\[CrossRef\]](#)
6. Antonov, V.A.; Davydov, A.A.; Firsov, K.N.; Gavrishchuk, E.M.; Kononov, I.G.; Kurashkin, S.V.; Podlesnykh, S.V.; Raspopov, N.A.; Zhavoronkov, N.V. Lasing characteristics of heavily doped single-crystal Fe:ZnSe. *Appl. Phys. B* **2019**, *125*, 173. [\[CrossRef\]](#)
7. Mirov, S.B.; Moskalev, I.S.; Vasilyev, S.; Smolski, V.; Fedorov, V.V.; Martyshkin, D.; Peppers, J.; Mirov, M.; Dergachev, A.; Gapontsev, V. Frontiers of mid-IR lasers based on transition metal doped chalcogenides. *IEEE J. Sel. Top. Quant.* **2018**, *24*, 1601829. [\[CrossRef\]](#)
8. Avetissov, I.; Chang, K.; Zhavoronkov, N.; Davydov, A.; Mozhevitina, E.; Khomyakov, A.; Kobeleva, S.; Neustroev, S. Non-stoichiometry and luminescent properties of ZnSe crystals grown from melt and vapor. *J. Cryst. Growth* **2014**, *401*, 686–690. [\[CrossRef\]](#)
9. Peppers, J.; Fedorov, V.V.; Mirov, S.B. Mid-IR photoluminescence of Fe²⁺ and Cr²⁺ ions in ZnSe crystal under excitation in charge transfer bands. *Opt. Express* **2015**, *23*, 4406–4414. [\[CrossRef\]](#)
10. Gladilin, A.A.; Gulyamova, E.S.; Danilov, V.P.; Il'ichev, N.N.; Kalinushkin, V.P.; Odin, I.N.; Pashinin, P.P.; Rezvanov, R.R.; Sidorin, A.V.; Studenikin, M.I.; et al. IR luminescence of Fe²⁺:ZnSe single crystals excited by an electron beam. *Quantum Electron.* **2016**, *46*, 545–547. [\[CrossRef\]](#)
11. Yang, G.; Jie, W.; Zhang, Q.Y. Photoluminescence investigation of CdZnTe: In single crystals annealed in CdZn vapors. *J. Mater. Res.* **2006**, *21*, 1807–1809. [\[CrossRef\]](#)
12. Tongay, S.; Suh, J.; Ataca, C.; Fan, W.; Luce, A.; Kang, J.S.; Liu, J.; Ko, C.; Raghunathanan, R.; Zhou, J.; et al. Defects activated photoluminescence in two-dimensional semiconductors: Interplay between bound, charged, and free excitons. *Sci. Rep.* **2013**, *3*, 2657. [\[CrossRef\]](#) [\[PubMed\]](#)

13. Kalinushkin, V.; Uvarov, O.; Mironov, S.; Nartov, K.; Il'ichev, N.; Studenikin, M.; Gavrischuk, E.; Timofeeva, N.; Rodin, S.; Gladilin, A. Influence of doping time on spatial distribution of luminescence intensity in ZnSe:Fe. *J. Lumin.* **2021**, *231*, 117795. [[CrossRef](#)]
14. Urbietta, A.; Fernandez, P.; Piqueras, J.; Munoz, V. Scanning electron microscopy characterization of ZnSe single crystals grown by solid-phase recrystallization. *Mat. Sci. Eng. B-Solid* **2000**, *78*, 105–108. [[CrossRef](#)]
15. Shu, S.W.; Ma, G.H. Temperature-dependent defect-induced new emission in ZnSe Crystal. *Chin. Phys. Lett.* **2009**, *26*, 047102. [[CrossRef](#)]
16. Li, H.Y.; Jie, W.Q.; Yang, L.; Zhang, S.A.; Sun, Z.R.; Xu, K.W. The structural damage and defects induced by femtosecond laser pulse in ZnSe single crystals. *Mat. Sci. Semicon. Proc.* **2006**, *9*, 151–155. [[CrossRef](#)]
17. Sushkevich, K.; Goncarenco, E.; Nedeoglo, N.; Nedeoglo, D. Photoluminescence of ZnSe samples doped with antimony and iodine. *Physica B* **2021**, *602*, 412466. [[CrossRef](#)]
18. Aminev, D.F.; Pruchkina, A.A.; Krivobok, V.S.; Gladilin, A.A.; Kalinushkin, V.P.; Ushakov, V.V.; Chentsov, S.I.; Onishchenko, E.E.; Kondrin, M.V. Optical marker of intrinsic point defects in ZnSe:Fe. *Opt. Mat. Express* **2021**, *11*, 210–218. [[CrossRef](#)]
19. Pruchkina, A.A.; Aminev, D.F.; Ushakov, V.V.; Chentsov, S.I.; Gladilin, A.A.; Krivobok, V.S.; Onishchenko, E.E.; Kalinushkin, V.P. Impurity- and defect-related luminescence of ZnSe:Fe at Low Temperatures. *Bull. Lebedev Phys. Inst.* **2019**, *46*, 238–242. [[CrossRef](#)]
20. Gladilin, A.; Chentsov, S.; Uvarov, O.; Nikolaev, S.; Krivobok, V.; Kalinushkin, V. Luminescence spatial characteristics of ZnSe:Fe. *J. Appl. Phys.* **2019**, *126*, 015702. [[CrossRef](#)]
21. Gladilin, A.A.; Il'ichev, N.N.; Kalinushkin, V.P.; Studenikin, M.I.; Uvarov, O.V.; Chapnin, V.A.; Tumorin, V.V.; Novikov, G.G. Study of the Effect of Doping with Iron on the Luminescence of Zinc-Selenide Single Crystals. *Semiconductors* **2019**, *53*, 1–8. [[CrossRef](#)]
22. Hizhnyi, Y.A.; Nedilko, S.G.; Borysiuk, V.I.; Chornii, V.P.; Rybalka, I.A.; Galkin, S.M.; Tupitsyna, I.A.; Klyui, N.I. Effect of annealing in zinc vapors on charge trapping properties of ZnSe, ZnSe(Te) and ZnSe(Al) scintillation crystals: Revealing the mechanisms by DFT computational studies. *Opt. Mater.* **2019**, *97*, 109402. [[CrossRef](#)]
23. Li, Y.X.; Yang, D.; Nan, W.N.; Zhang, L.; Yu, H.W.; Zhou, B.R.; Hu, Z.G. The crystal growth of ZnSe by the traveling heater method with the accelerated crucible rotation technique. *J. Cryst. Growth* **2022**, *589*, 126684. [[CrossRef](#)]
24. Kannappan, P.; Falcao, B.P.; Asokan, K.; Leitao, J.P.; Dhanasekaran, R. Insights into recombination channels in a CVT grown ZnSe single crystal. *Appl. Phys. A* **2022**, *128*, 114. [[CrossRef](#)]
25. Zázvorka, J.; Hlíděk, P.; Grill, R.; Franc, J.; Belas, E. Photoluminescence of CdTe:In the spectral range around 1.1 eV. *J. Lumin.* **2016**, *177*, 71–81. [[CrossRef](#)]
26. Il'ichev, N.N.; Bufetova, G.A.; Gulyamova, E.S.; Pashinin, P.P.; Sidorin, A.V.; Kalinushkin, V.P.; Tumorin, V.V.; Gladilin, A.A. Nonlinear transmittance of a diffusion-doped single crystal ZnSe:Fe²⁺ at a wavelength of 2940 nm at low and room temperature. *Laser Phys.* **2019**, *29*, 025002. [[CrossRef](#)]
27. Wang, X.; Chen, Z.; Zhang, L.; Jiang, B.; Xu, M.; Hong, J.; Wang, Y.; Zhang, P.; Zhang, L.; Hang, Y. Preparation, spectroscopic characterization and energy transfer investigation of iron-chromium diffusion co-doped ZnSe for mid-IR laser applications. *Opt. Mater.* **2016**, *54*, 234–237. [[CrossRef](#)]
28. Suganthi, N.; Pushpanathan, K. Spherical and dumbbell shape biphasic paramagnetic ZnS:Fe nanoparticles on ferromagnetic ZnS host background. *J. Electron. Mater.* **2018**, *47*, 7343–7357. [[CrossRef](#)]
29. Yang, L.; Zhu, J.G.; Xiao, D.Q. Microemulsion-mediated hydrothermal synthesis of ZnSe and Fe-doped ZnSe quantum dots with different luminescence characteristics. *RSC Adv.* **2012**, *2*, 8179–8188. [[CrossRef](#)]
30. Li, T.T.; Sun, C.C.; Xue, C.; Jiang, Y.T.; Zhang, J.; Zhao, L.J. Structure and optical properties of iron doped ZnSe microspheres. *Opt. Mater.* **2021**, *114*, 110989. [[CrossRef](#)]
31. Yamashita, T.; Hayes, P. Analysis of XPS spectra of Fe²⁺ and Fe³⁺ ions in oxide materials. *Appl. Surf. Sci.* **2008**, *254*, 2441–2449. [[CrossRef](#)]
32. Saxena, A.; Yang, S.X.; Philipose, U.; Ruda, H.E. Excitonic and pair-related photoluminescence in ZnSe nanowires. *J. Appl. Phys.* **2008**, *103*, 053109. [[CrossRef](#)]
33. Kulyuk, L.L.; Laiho, R.; Lashkul, A.V.; Lahderanta, E.; Nedeoglo, D.D.; Nedeoglo, N.D.; Radevici, I.V.; Siminel, A.V.; Sirkeli, V.P.; Sushkevich, K.D. Magnetic and luminescent properties of iron-doped ZnSe crystals. *Physica B* **2010**, *405*, 4330–4334. [[CrossRef](#)]
34. Surma, M.; Godlewski, M.; Surkova, T. Iron and chromium impurities in ZnSe as centers of nonradiative recombination. *Phys. Rev. B* **1994**, *50*, 8319. [[CrossRef](#)] [[PubMed](#)]
35. Dean, P.; Herbert, D.; Werkhoven, C.; Fitzpatrick, B.; Bhargava, R. Donor bound-exciton excited states in zinc selenide. *Phys. Rev. B* **1981**, *23*, 4888. [[CrossRef](#)]
36. Dean, P.; Fitzpatrick, B.; Bhargava, R. Optical properties of ZnSe doped with Ag and Au. *Phys. Rev. B* **1982**, *26*, 2016. [[CrossRef](#)]
37. Tournie, E.; Neu, G.; Teisseire, M.; Faurie, J.P.; Pelletier, H.; Theys, B. Spectroscopy of the interaction between nitrogen and hydrogen in ZnSe epitaxial layers. *Phys. Rev. B* **2000**, *62*, 12868–12874. [[CrossRef](#)]
38. Colibaba, G.V.; Nedeoglo, D.D.; Ursaki, V.V. Impurity centers in ZnSe:Na crystals. *J. Lumin.* **2011**, *131*, 1966–1970. [[CrossRef](#)]
39. Neu, G.; Tournie, E.; Morhain, C.; Teisseire, M.; Faurie, J.P. Spectroscopy of the phosphorus impurity in ZnSe epitaxial layers grown by molecular-beam epitaxy. *Phys. Rev. B* **2000**, *61*, 15789–15796. [[CrossRef](#)]
40. Worschech, L.; Ossau, W.; Fischer, C.; Schäfer, H.; Landwehr, G. Characterization of structural defects in MBE grown ZnSe. *Mater. Sci. Eng. B* **1997**, *43*, 29–32. [[CrossRef](#)]
41. Dean, P.J.; Pitt, A.D.; Skolnick, M.S.; Wright, P.J.; Cockayne, B. Optical properties of undoped organometallic grown ZnSe and ZnS. *J. Cryst. Growth* **1982**, *59*, 301–306. [[CrossRef](#)]

42. Zhang, Y.; Skromme, B.; Shibli, S.; Tamargo, M. Properties of the As-related shallow acceptor level in heteroepitaxial ZnSe grown by molecular-beam epitaxy. *Phys. Rev. B* **1993**, *48*, 10885. [[CrossRef](#)] [[PubMed](#)]
43. Nelkowski, H.; Pfützenreuter, O.; Schrittenlacher, W. Comparison of luminescence- and ESR-investigations in ZnS:Fe. *J. Lumin.* **1979**, *20*, 403–408. [[CrossRef](#)]
44. Podlowski, L.; Heitz, R.; Thurian, P.; Hoffmann, A.; Broser, I. Nonradiative transition rates of Fe²⁺ in III–V and II–VI semiconductors. *J. Lumin.* **1994**, *58*, 252–256. [[CrossRef](#)]

Disclaimer/Publisher’s Note: The statements, opinions and data contained in all publications are solely those of the individual author(s) and contributor(s) and not of MDPI and/or the editor(s). MDPI and/or the editor(s) disclaim responsibility for any injury to people or property resulting from any ideas, methods, instructions or products referred to in the content.